RESEARCH ARTICLE

National Science Review
0: nwad149, 2023
https://doi.org/10.1093/nsr/nwad149
Advance access publication 23 May 2023

MATERIALS SCIENCE

Confinement of ionomer for electrocatalytic CO_2 reduction reaction via efficient mass transfer pathways

Xiaowei Du[1,2,†], Peng Zhang[1,2,4,†], Gong Zhang[1,2], Hui Gao[1,2], Lili Zhang[1,2], Mengmeng Zhang[1,2], Tuo Wang[1,2,4,5] and Jinlong Gong[1,2,3,4,*]

[1]School of Chemical Engineering and Technology, Key Laboratory for Green Chemical Technology of the Ministry of Education, Tianjin University, Tianjin 300072, China; [2]Collaborative Innovation Center of Chemical Science and Engineering (Tianjin), Tianjin 300072, China; [3]Haihe Laboratory of Sustainable Chemical Transformations, Tianjin 300192, China; [4]National Industry-Education Platform of Energy Storage, Tianjin University, Tianjin 300350, China and [5]Joint School of the National University of Singapore and Tianjin University, International Campus of Tianjin University, Fuzhou 350207, China

***Corresponding author.** E-mail: jlgong@tju.edu.cn

[†]Equally contributed to this work.

Received 28 March 2023; **Accepted** 21 May 2023

ABSTRACT

Gas diffusion electrodes (GDEs) mediate the transport of reactants, products and electrons for the electrocatalytic CO_2 reduction reaction (CO_2RR) in membrane electrode assemblies. The random distribution of ionomer, added by the traditional physical mixing method, in the catalyst layer of GDEs affects the transport of ions and CO_2. Such a phenomenon results in elevated cell voltage and decaying selectivity at high current densities. This paper describes a pre-confinement method to construct GDEs with homogeneously distributed ionomer, which enhances mass transfer locally at the active centers. The optimized GDE exhibited comparatively low cell voltages and high CO Faradaic efficiencies (FE > 90%) at a wide range of current densities. It can also operate stably for over 220 h with the cell voltage staying almost unchanged. This good performance can be preserved even with diluted CO_2 feeds, which is essential for pursuing a high single-pass conversion rate. This study provides a new approach to building efficient mass transfer pathways for ions and reactants in GDEs to promote the electrocatalytic CO_2RR for practical applications.

Keywords: CO_2 electroreduction, gas diffusion electrode, mass transfer, ionomer, Ag catalyst

INTRODUCTION

The electrocatalytic CO_2 reduction reaction (CO_2RR) is an eminently attractive technology for converting CO_2 into value-added products using renewable energy (e.g. solar and wind energy) [1–4]. To meet the requirements of industrial applications, it is necessary to develop efficient electrolyzers [5,6]. Membrane electrode assemblies (MEAs) based on gas diffusion electrodes (GDEs) have been widely studied in recent years [7]. The configuration of the MEA not only overcomes the mass transfer limitations in the H-cell but also eliminates the use of cathode electrolyte to mitigate the full cell resistance and improve stability [8,9]. GDEs, as one of the important components in the MEA, are porous electrodes that support catalysts. Generally, a GDE consists of a catalyst layer (CL) and a gas diffusion layer (GDL) [10–12]. The CL is the main place for the catalytic reaction, which normally includes the catalyst to provide the active centers, the catalyst carrier serving as the support, and the ionomer. The ionomer, composed of polymer backbones and hydrophilic groups [13–15], affects the transport of ions and reactants at the catalyst surface, thus impacting the performance of the GDEs [16,17]. Therefore, the ionomer plays an important role during catalytic processes. In order to enhance the electrocatalytic CO_2RR, the ionomer in the CL should be better homogeneously distributed, which can both prevent catalyst agglomeration and ensure rapid mass transfer [17,18].

Normally, there are two main ways of adding the ionomer to the CL. One is the coating of ionomer onto the CL, which is carried out via ink-free methods (e.g. electrodeposition, sputter and ion-beam deposition approaches) [19–22]. However, the inhomogeneous distribution of the ionomer only on the surface of the CL increases ion transport resistance, leading to deteriorated catalytic performance. The other way of adding the ionomer to the CL is via physical mixing of ionomer into the catalyst ink, which is then coated onto the GDL mainly through drop-casting, hand-painting or spray-coating processes [23,24]. Ink-based approaches are widely

adopted due to their advantages of simplicity, flexibility and scalability, which are more suitable for particle catalysts [19,23,25]. However, due to the weak interaction between the catalyst and ionomer in the ink, GDEs obtained by these methods suffer from the random distribution of ionomer. Ionomer aggregation at certain positions in a GDE would lead to high local resistance to mass transfer. At the same time, active centers that are not covered by ionomer might not function properly due to the lack of ion transfer paths [10,26–28]. Thus, effective regulation of the homogeneity of ionomer is essential to promote catalytic performance.

Uniform distribution of ionomer could be achieved by tuning the solvent used in the catalyst ink. Berlinguette *et al.* found that the use of ethanol as ink solvent would facilitate moderate aggregation of ionomer, which in turn optimized its presence in the CL [29]. The obtained GDE possessed promoted selectivity of CO. Improving the interaction between the catalyst carrier and the ionomer can alleviate the aggregation of the ionomer. Strasser *et al.* proposed that the introduction of pyridine/pyrrole functional groups containing N elements on catalyst carriers enhanced their interaction with ionomer. This method promoted the spatial distribution of the ionomer, which improved the efficiency of catalyst utilization and increased the power density of the GDEs [27]. In addition, the optimized allocation of ionomer can be achieved by the modification of ionomer. Yan *et al.* tuned the electrostatic repulsion in the ionomer by optimizing the spacing distance of cationic groups in the ionomer backbone, which regulates the electrostatic repulsion and Van der Waals forces between the ionomer and catalyst. This method prevented the agglomeration of catalyst particles by promoting the distribution of ionomer within the CL, and improved the catalytic activity [17]. Despite the efforts devoted to tuning the presence of ionomer, a more proactive and controllable approach is still needed to further optimize the distribution of ionomer to achieve good performance for the practical application of CO_2RR systems.

Although there are a lot of works carried out on GDEs modification nowadays, those electrodes made by spraying still suffer from non-uniform distribution of ionomer. Herein, an ionomer pre-confinement method is developed. Specifically, ionomer was introduced during the synthetic process of electrocatalysts, leading to the formation of ionomer-confined electrocatalysts for the construction of GDEs. This method improves the homogeneity of ionomer distribution, building efficient mass transfer pathways. On the one hand, it makes the distribution of pores on the GDEs more average and avoids the high local mass transfer resistance caused by ionomer accumulation, which enhances CO_2 transport and improves the catalytic performance. On the other hand, it also ensures the successful occurrence of the reaction at the catalytic site and facilitates ion transport within the CL. The promoted CO_2 mass transfer would lead to a high CO Faradaic efficiency (FE) of over 90% even at a high current density of 600 mA cm^{-2}. The enhanced ion transport could result in a decrease in cell voltage ($\sim$3.3 V at 300 mA cm^{-2}). In addition, these optimizations also enable the preservation of high selectivity at relatively low CO_2 concentrations. The optimized electrodes also achieve stable catalysis at a current density of 300 mA cm^{-2} for >220 h.

RESULTS AND DISCUSSION

Synthesis and structural characterization of Ag@ionomer and Ag/ionomer catalysts

Pre-confinement of ionomer was realized by adding PiperION-A5-HCO_3 anion exchange resin during the synthesis of Ag through the traditional colloidal method (see the Supplementary Data for more details) [30,31]. The electrocatalyst obtained after drying at room temperature is defined as Ag@ionomer (Fig. 1a and Supplementary Fig. 1a). The control sample prepared by physically mixing the ionomer and Ag particles (synthesized by the colloidal method [32], Supplementary Figs 1b and 2) is defined as Ag/ionomer. The Ag@ionomer and Ag/ionomer samples possess similar Ag particle sizes mainly due to the use of the same strong reductant and stabilizer [33,34]. A thin layer of ionomer around the Ag particles can be observed in the transmission electron microscope (TEM) images of Ag@ionomer (Fig. 1b and c). The electron dispersive X-ray spectroscopy (EDS) mappings also demonstrate the uniform distribution of ionomer around the catalyst (Fig. 1d). In addition, the Fourier transformed infrared spectroscopy (FT-IR) spectrum of Ag@ionomer shows peaks consistent with pure ionomer (Fig. 1e), revealing the presence of ionomer in its intrinsic form in the Ag@ionomer. X-ray diffraction (XRD) and X-ray photoelectron spectroscopy (XPS) results indicate that the ionomer does not affect the physicochemical properties of Ag (Fig. 1f and g). Thermogravimetric analysis (TGA) shows that Ag@ionomer and Ag/ionomer possess similar contents of ionomer (i.e. 15 wt%, Supplementary Fig. 3). Differential thermal analysis (DTA) reveals that Ag@ionomer has a higher decomposition temperature than Ag/ionomer and pure ionomer (Fig. 1h). The similar decomposition temperatures of Ag/ionomer and ionomer may be due to the fact that Ag/ionomer

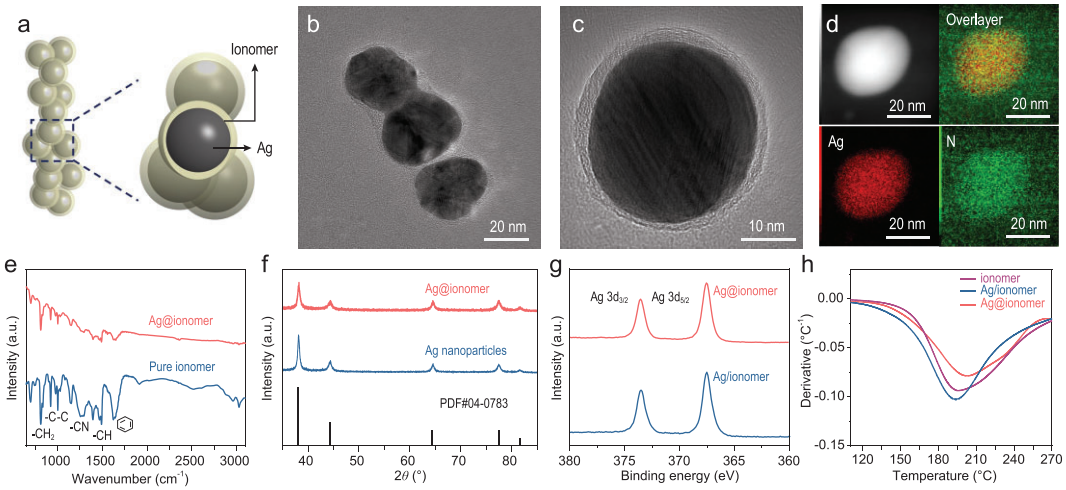

Figure 1. (a) Schematic illustration of the Ag@ionomer. (b and c) TEM images of Ag@ionomer. (d) High-angle annular dark-field scanning transmission electron microscopy image and EDS mapping images of Ag@ionomer. (e) FT-IR spectrum of pure ionomer and Ag@ionomer. (f) XRD patterns of the Ag nanoparticles and Ag@ionomer. (g) XPS spectra of the Ag/ionomer and Ag@ionomer. (h) DTA of ionomer, Ag/ionomer and Ag@ionomer.

is prepared by physical mixing, which leads to only weak interaction by van der Waals force between Ag and ionomer. The higher decomposition temperature indicates the strong interaction between the catalyst and the ionomer in the pre-confined Ag@ionomer electrocatalyst [35,36].

Fabrication and activity evaluation of $GDE_{Ag@ionomer}$ and $GDE_{Ag/ionomer}$

Subsequently, different GDEs were prepared by airbrushing varied catalyst inks onto carbon GDLs (Supplementary Fig. 4). $GDE_{Ag@ionomer}$ and $GDE_{Ag/ionomer}$ were prepared using the inks with Ag@ionomer and Ag/ionomer dissolved in a mixed solution of isopropyl alcohol and water, respectively (Supplementary Fig. 5). The electrocatalytic performance of the cells was tested in a 4 cm^2 MEA at room temperature (~25°C) in the galvanostatic mode (Fig. 2a) [37]. The products were analyzed by gas chromatography (GC). According to the results of activity tests for $GDE_{Ag@ionomer}$ and $GDE_{Ag/ionomer}$ with different contents of ionomer (Fig. 2 and Supplementary Figs 6–8), the optimal CO_2RR performance is achieved when the ionomer content is moderate (~15 wt%), with the thickness of the ionomer layer on the catalyst surface being ~1.5 nm (Supplementary Fig. 9). The tests of GDEs with optimized ionomer content indicate that $GDE_{Ag@ionomer}$ exhibits a lower cell voltage and higher energy efficiency than $GDE_{Ag/ionomer}$ (Fig. 2b and c). In addition to the relatively low cell voltage, $GDE_{Ag@ionomer}$ also possesses a higher selectivity towards CO (over 90% even at 600 mA cm^{-2}) than the $GDE_{Ag/ionomer}$ (Fig. 2d and e). In order to confirm the source of the products, the composition of CO_2 feedstock was first checked. The results showed that the feedstock only contained CO_2 (Supplementary Fig. 10). Subsequently, a control experiment under Ar atmosphere was conducted (Supplementary Fig. 11). When the Ar atmosphere was used, it was found that no carbon-based species were produced. Therefore, it can be determined that CO is generated by the reduction of CO_2. The stability of the GDEs was tested at a constant current density of 300 mA cm^{-2} (Fig. 2f and Supplementary Fig. 12). In this process, a humidified CO_2 feedstock with a relative humidity of ~100% was used, which means that the CO_2 first passed through a humidification tank containing ultrapure water (at ~25°C) before being fed into the reactor. In the stability test, $GDE_{Ag@ionomer}$ achieved stable operation for >220 h with the FE for CO maintained above 75%. The full cell voltage kept constant at ~3.2 V with a full cell energy efficiency of ~32% (Fig. 2f). The CO FE first decreased and then became constant, which is probably due to the water management problem [38–40]. As the reaction proceeds, the generation of salt on the electrodes due to the locally generated OH^- makes the electrode progressively hydrophilic (Supplementary Fig. 13). Thus, the electrode becomes over humidified and hydrogen-evolution-reaction (HER) dominated, leading to the decrease of CO FE. Subsequently, the water mass transfer in the reactor reached a balanced state, which in turn maintained the CO FE at a certain level without further decrease. In response to this problem, further investigations (e.g. hydrothermal management of the reaction system, anodic gaseous

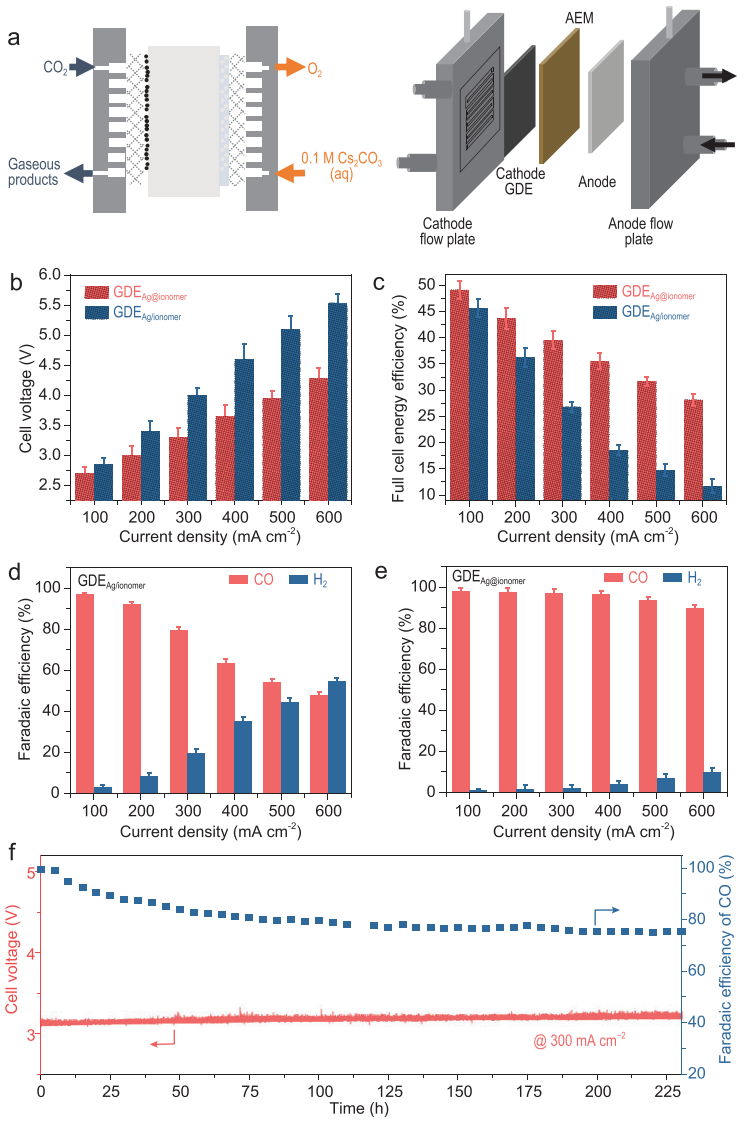

Figure 2. (a) 2D and 3D views of the MEA electrolyzer. (b and c) Cell voltages and full cell energy efficiencies of MEAs with $GDE_{Ag@ionomer}$ and $GDE_{Ag/ionomer}$ as the GDE at different current densities. FEs for CO and H_2 over (d) $GDE_{Ag/ionomer}$ and (e) $GDE_{Ag@ionomer}$ in the MEA. (f) Stability test of $GDE_{Ag@ionomer}$ at a current density of 300 mA cm^{-2}.

reactant oxidation) are needed in the future to achieve better system stability. Furthermore, no morphological or structural change was observed for the GDEs after the stability tests (Fig. 3a–d and Supplementary Fig. 14).

To examine whether the prevention of aggregation in Ag@ionomer is the key, an Ag+ionomer sample was prepared by adding ionomer after the reduction of the silver precursor in a typical synthesis of Ag nanoparticles before the centrifugation. In Ag+ionomer, Ag nanoparticles and ionomer are segregated with weak interaction (Supplementary Fig. 15). At the same time, the Ag nanoparticles are well dispersed without aggregation. The performance of $GDE_{Ag+ionomer}$ was far worse than that of the $GDE_{Ag@ionomer}$, which is comparable with that of the $GDE_{Ag/ionomer}$ (Supplementary Fig. 16). These results suggest that the prevention of aggregation in the Ag@ionomer may not be the main reason for its improved performance.

The good performance of $GDE_{Ag@ionomer}$ may be ascribed to the uniform distribution of ionomer as a result of the pre-confinement method. Homogeneously distributed ionomer in the CL may provide more efficient ion transport paths and facilitate the transfer of ions generated at the reaction sites to the anode, which would reduce cell voltage and increase full cell energy efficiency. In addition, the transfer of CO_2 could be promoted by avoiding local mass transfer resistance caused by ionomer accumulation. This phenomenon would allow easy access for CO_2 at the active sites and improve the local CO_2 concentration [41]. CO_2 surface coverage of the catalyst is directly related to the local CO_2 concentration, which enhances the selectivity of CO at high current densities.

Structural characterization of $GDE_{Ag@ionomer}$ and $GDE_{Ag/ionomer}$

In order to verify this hypothesis, we first exclude the possibility that the intrinsic activities of the Ag electrocatalyst in $GDE_{Ag@ionomer}$ and $GDE_{Ag/ionomer}$ are different by Tafel analysis (Supplementary Figs 17 and 18, and Supplementary Table 1) [42,43]. The almost identical exchange current density and Tafel slopes of these two electrodes can provide comparable kinetic data, which indicates that the improvement of the catalytic performance of $GDE_{Ag@ionomer}$ could be attributed to the structural benefits [44–46]. As revealed by a scanning electron microscope (SEM), the $GDE_{Ag@ionomer}$ electrode has a more pronounced porous structure than the $GDE_{Ag/ionomer}$ (Fig. 3a–d), which may be explained by the uniform distribution of ionomer in the $GDE_{Ag@ionomer}$. To better reveal the distribution of ionomer within the CL, focused ion beam SEM (FIB-SEM) characterization with EDS mapping was performed (Fig. 3e and f, and Supplementary Fig. 19) [47]. The results show that $GDE_{Ag@ionomer}$ reserves the porous structure throughout the CL without significant ionomer aggregation, while the ionomer accumulates at the surface of $GDE_{Ag/ionomer}$. The optimized ionomer distribution in $GDE_{Ag@ionomer}$ can also be reflected by the pore size distributions of the electrodes [48]. As revealed by mercury intrusion porosimetry (MIP) experiments (Supplementary Fig. 20) [49], $GDE_{Ag@ionomer}$ has a more concentrated pore size distribution than $GDE_{Ag/ionomer}$. The mutual verification between the results of MIP and FIB-SEM

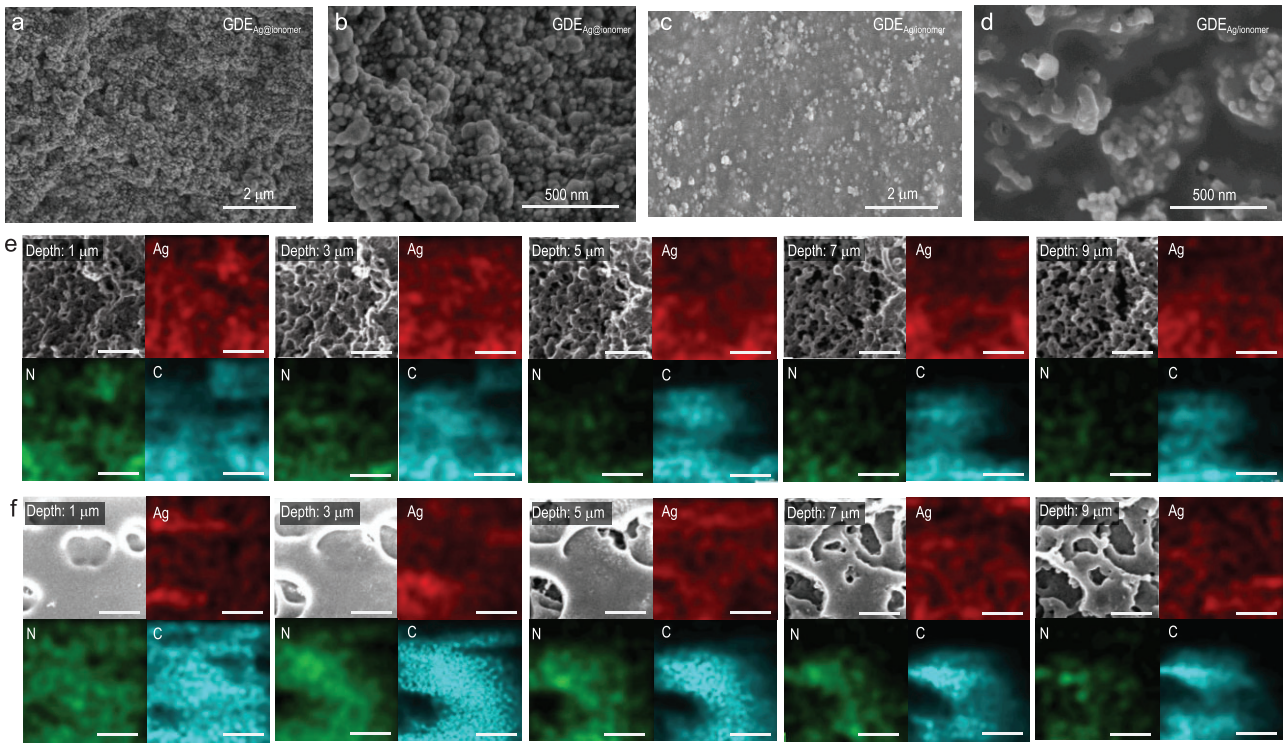

Figure 3. SEM images of (a and b) GDE$_{Ag@ionomer}$ and (c and d) GDE$_{Ag/ionomer}$. FIB-SEM and corresponding EDS mapping images (scale bars: 2 μm) of (e) GDE$_{Ag@ionomer}$ and (f) GDE$_{Ag/ionomer}$.

shows that homogeneous distribution of ionomer in GDE$_{Ag@ionomer}$ avoids the blocking of pores caused by the enrichment of ionomer at the surface of GDE$_{Ag/ionomer}$.

Promoting mechanism of uniformly distributed ionomer in GDE$_{Ag@ionomer}$

The structural characterizations above show that this GDE using the ionomer-confined electrocatalyst optimizes the distribution of ionomer within the CL, building effective ion paths around the catalytic sites (Fig. 4a). To prove that the uniformly distributed ionomer would enhance the ion transport, electrochemical impedance spectroscopy (EIS) tests were performed under operating conditions. The equivalent circuit to which the EIS data were adapted is shown in Fig. 4b, where R_s represents internal resistance, R_{CT}^{Total} represents charge transfer resistance, C_{dl}^{Total} represents the sum of cathode and anode electrode capacitance, and R_d represents Nernst diffusion impedance [50]. The values of the components in the equivalent circuit are shown in Supplementary Table 2. The high-frequency impedance is obtained by measuring across the entire cell in the two-electrode mode, where the difference is considered to be possibly derived from the cathode part [51]. The results indicate that GDE$_{Ag@ionomer}$ has a lower charge transfer resistance and a lower diffusion impedance than GDE$_{Ag/ionomer}$ (Fig. 4b). With regard to the electron transfer within the GDE$_{Ag@ionomer}$, the negative effect of the ionomer distributed around the catalyst on the electron transfer cannot be denied. However, when there is a thin ionomer layer between catalysts, electrons can still be conducted through a tunneling effect [52,53]. In addition, the catalysts are not completely isolated from each other, which provides pathways for electron transport within the catalyst layer (Fig. 1b). Therefore, the electron transport probably has a minor effect on the successful occurrence of the reaction within the CL. The relatively low diffusion impedance indicates a rapid transfer of reactants and products in the GDE$_{Ag@ionomer}$. Since the ions were generated during the electrochemical CO_2RR, the well-dispersed ionomer within the CL could facilitate ion transport to reduce the resistance of its diffusion processes [17,51].

In order to prove that the homogeneous distribution of ionomer in the CL can reduce the mass transfer resistance of CO_2, an activity evaluation using CO_2 feeds diluted with inert Ar (with CO_2 concentration down to 20 vol%, see the Supplementary Data for more details) was performed. With a decrease of CO_2 concentration to 40 vol%, no significant degradation of CO FE was observed for

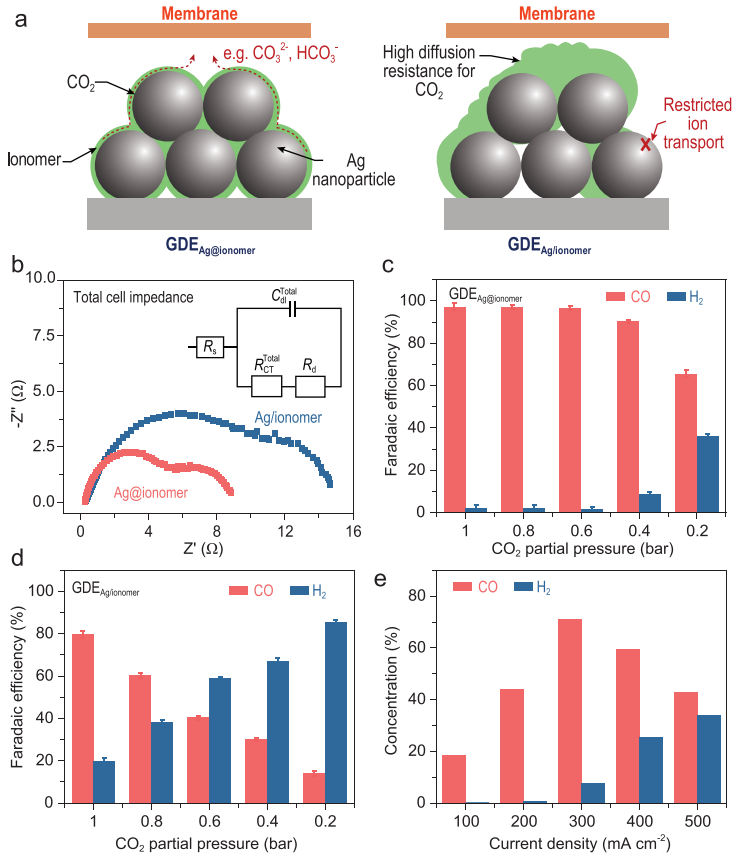

Figure 4. (a) Schematic diagram of the $GDE_{Ag@ionomer}$ and $GDE_{Ag/ionomer}$. (b) Nyquist plots of the impedance related to the electrode. (c and d) Effect of CO_2 partial pressure on the CO_2RR performance of $GDE_{Ag/ionomer}$ (c) and $GDE_{Ag@ionomer}$ (d). (e) FEs for CO and H_2 over $GDE_{Ag@ionomer}$ in the tandem reactor system at different current densities.

$GDE_{Ag@ionomer}$ at a current density of 300 mA cm^{-2} (Fig. 4c). The CO FE of $GDE_{Ag@ionomer}$ is still ~70% when the CO_2 concentration is reduced to 20 vol%. However, the CO FE of $GDE_{Ag/ionomer}$ showed a rapid decreasing trend (Fig. 4d). These results indicate that the homogeneous distribution of ionomer around the catalyst reduces the mass transfer resistance of CO_2 and improves the utilization efficiency of the active sites. A slight increase in cell voltage can be noticed with a decrease in CO_2 concentration (Supplementary Fig. 21). For further proof of the enhanced CO_2 mass transfer, the concentration of CO_2 within the CL was tracked based on a reaction-diffusion model (Supplementary Fig. 22, see the Supplementary Data for more details). Based on the test results of FIB-SEM and SEM, two porous models with different pore distributions were established to represent the CLs. The $GDE_{Ag@ionomer}$ model exhibits a higher local CO_2 concentration than $GDE_{Ag/ionomer}$ after providing the models with the same CO_2 feedstock and current density, which indicates that a more uniform pore distribution facilitates CO_2 transport within the CL. Therefore, this result further proves that the electrode with uniform distribution of ionomer made by the pre-confinement method has lower mass transfer resistance, promoting the mass transfer of CO_2 within the CL and increasing the local CO_2 concentration.

Based on the good performance of $GDE_{Ag@ionomer}$ at low CO_2 concentrations, a tandem reactor system was built to improve the single-pass conversion of CO_2. By connecting three MEAs in series, the highest outlet concentration of CO is nearly 71 vol% at a current density of 300 mA cm^{-2} (Fig. 4e). The cell voltages of the three reactors are almost identical at the same current density (Supplementary Fig. 23). To evaluate the universality of this method, another ionomer, i.e. Fumion FAA-3, was examined using this pre-confinement method. During the activity test, the ion exchange membrane was replaced with the matching FAA-3–50. According to the results of activity evaluation (Supplementary Fig. 24), the obtained electrode ($GDE_{Ag@ionomer\ (FAA)}$) also exhibited promoted activity compared with that prepared by the conventional method ($GDE_{Ag/ionomer\ (FAA)}$). This pre-confinement method has the potential to be adopted by more systems.

CONCLUSION

In summary, a pre-confinement method is developed to construct GDEs with homogeneously distributed ionomer in the CL for enhancing mass transfer during the electrochemical CO_2RR. The uniform ionomer builds paths for the promoted transport of ions, leading to reduced cell voltage, which also facilitates the mass transfer of CO_2. As a result, easy access to CO_2 at the active centers would contribute to a high CO FE of over 90% even at a high current density of 600 mA cm^{-2}, with the ability to achieve high CO_2 conversion rates. Moreover, the obtained $GDE_{Ag@ionomer}$ exhibited good stability for more than 220 h at a current density of 300 mA cm^{-2}. Considering the high energy conversion efficiency, the high CO FE at high current densities and the good stability, this $GDE_{Ag@ionomer}$ has the potential to realize the electrochemical CO_2RR in practical applications.

METHODS

Materials

$AgNO_3$ (99.8%) and NaOH (99%) were purchased from Aladdin Industrial Co. Ltd. Cs_2CO_3 (99.9%), isopropyl alcohol (≥99.5%) and ethanol (HPLC, ≥99.8%) were purchased from Macklin Biochemical Co. Ltd. Sodium citrate anhydrous (99%) was

purchased from J&K Scientific Ltd. L (+) − Ascorbic acid (≥99.7%) was purchased from Tianjin Kemiou Chemical Reagent Co. Ltd. All chemical reagents were utilized without further purification. Commercially available carbon-based GDLs (AvCarb GDS3250) were purchased from Xima Laya Photo-Electric Technology Co. Ltd., China. PiperION-A5-HCO_3 anion exchange resin, Fumion FAA anion exchange resin, PiperION-A15-HCO_3 and FAA-3-50 were purchased from SCI Materials Hub. CO_2, N_2, Ar and H_2 were all purchased from Air Liquide (≥99.999%). The ultrapure water (18.25 MΩ·cm) was supplied by a Millipore Direct-Q5 UV water purification system.

Catalyst synthesis

Ag nanoparticles were synthesized by using L (+) − Ascorbic acid as the reductant and sodium citrate anhydrous as the stabilizer [32]. Ag@ionomer nanoparticles were prepared under the same conditions. The difference was that 0.045 g of PiperION anion exchange resin was first dissolved in 30 mL of ethanol and mixed with the $AgNO_3$ solution before being added to the reducing agent solution.

Fabrication of electrodes

For the preparation of electrodes, 65 mg of Ag nanoparticles with 0.23 g of 5 wt% ionomer solution were dispersed in 4 mL of isopropyl alcohol and 4 mL of water to form Ag catalyst ink. After 1 h of sonication, the catalyst ink was sprayed onto 25 cm^2 carbon paper to fabricate $GDE_{Ag/ionomer}$. $GDE_{Ag@ionomer}$ was also prepared in a similar manner with the catalyst ink consisting of 65 mg of Ag@ionomer catalyst, 4 mL of isopropyl alcohol and 4 mL of water. During the preparation of GDEs, a hotplate and infrared lamp were used to accelerate the evaporation of the solvent.

CO_2RR performance test in the MEA

The homemade 4 cm^2 MEA (Gaossunion Co. Ltd.) consists of a GDE, an anion exchange membrane (PiperION-A15-HCO_3, SCI Materials Hub) and an IrRu/Ti anode. The PiperION ion-exchange membrane (15 μm, without polytetrafluoroethylene (PTFE)-reinforced) was mounted between a cathode GDE and an IrRu-coated Ti mesh anode, with the CL of the GDE oriented towards the membrane [35]. During the testing process, 0.1 M Cs_2CO_3 solution served as the anolyte and the humidified CO_2 flow (relative humidity ∼100%), controlled by the mass flow meter, was supplied to the cathode which had an inlet flow rate controlled at 50 sccm. Since CO_2 at the cathode can react with OH^- to form HCO_3^-/CO_3^{2-}, another mass flow meter was used to detect the outlet gas flow rate in order to ensure the accuracy of the gas product selectivity calculation. A fresh GDE, IrRu/Ti anode and anion exchange membrane were used for each electrocatalytic test.

Characterization

The phase structures were characterized by XRD (Bruker, D8-Focus, Cu Kα radiation) at 40 kV and 40 mA. SEM micrographs were acquired using a Hitachi S-4800 focused ion beam SEM with an accelerating voltage of 5 kV. TEM images were taken on a JEOL JEM-2100F operated at an acceleration voltage of 200 kV. XPS measurements were performed on a Physical Electronics PHI 1600 ESCA system with an excitation source of Al Kα = 1486.6 eV.

SUPPLEMENTARY DATA

Supplementary data are available at *NSR* online.

FUNDING

This work was supported by the National Key R&D Program of China (2021YFA1501503), the National Natural Science Foundation of China (22121004, 22038009, 22250008 and 22108197), the Haihe Laboratory of Sustainable Chemical Transformations (CYZC202107), the Program of Introducing Talents of Discipline to Universities (BP0618007) and the Xplorer Prize.

AUTHOR CONTRIBUTIONS

J.G. supervised the research. X.D., P.Z. and J.G. conceived the ideas and designed the experiments. X.D., G.Z., H.G. and M.Z. performed the experiments, device fabrication, electrochemical measurements, materials characterization and data analysis. L.Z. performed the mass transport simulations. X.D., P.Z., and J.G. wrote the manuscript. All authors discussed the experiments and commented on the manuscript.

Conflict of interest statement. None declared.

REFERENCES

1. Deng W, Zhang L and Dong H *et al.* Achieving convenient CO_2 electroreduction and photovoltage in tandem using potential-insensitive disordered Ag nanoparticles. *Chem Sci* 2018; **9**: 6599–604.
2. Chang X, Wang T and Gong J. CO_2 photo-reduction: insights into CO_2 activation and reaction on surfaces of photocatalysts. *Energy Environ Sci* 2016; **9**: 2177–96.
3. Ling Y, Ma Q and Yu Y *et al.* Optimization strategies for selective CO_2 electroreduction to fuels. *Trans Tianjin Univ* 2021; **27**: 180–200.

4. Gao Z, Li J and Zhang Z *et al.* Recent advances in carbon-based materials for electrochemical CO_2 reduction reaction. *Chin Chem Lett* 2022; **33**: 2270–80.
5. Masel RI, Liu Z and Yang H *et al.* An industrial perspective on catalysts for low-temperature CO_2 electrolysis. *Nat Nanotechnol* 2021; **16**: 118–28.
6. Guo H, Si D-H and Zhu H-J *et al.* Ni single-atom sites supported on carbon aerogel for highly efficient electroreduction of carbon dioxide with industrial current densities. *eScience* 2022; **2**: 295–303.
7. Lees EW, Mowbray BAW and Parlane FGL *et al.* Gas diffusion electrodes and membranes for CO_2 reduction electrolysers. *Nat Rev Mater* 2021; **7**: 55–64.
8. Weekes DM, Salvatore DA and Reyes A *et al.* Electrolytic CO_2 reduction in a flow cell. *Acc Chem Res* 2018; **51**: 910–8.
9. Chen C, Li Y and Yang P. Address the 'alkalinity problem' in CO_2 electrolysis with catalyst design and translation. *Joule* 2021; **5**: 737–42.
10. Lees EW, Mowbray BAW and Salvatore DA *et al.* Linking gas diffusion electrode composition to CO_2 reduction in a flow cell. *J Mater Chem A* 2020; **8**: 19493–501.
11. Khedekar K, Satjaritanun P and Stewart S *et al.* Effect of commercial gas diffusion layers on catalyst durability of polymer electrolyte fuel cells in varied cathode gas environment. *Small* 2022; **18**: e2201750.
12. Wang K, Liu D and Liu L *et al.* Tuning the local electronic structure of oxygen vacancies over copper-doped zinc oxide for efficient CO_2 electroreduction. *eScience* 2022; **2**: 518–28.
13. Salvatore DA, Gabardo CM and Reyes A *et al.* Designing anion exchange membranes for CO_2 electrolysers. *Nat Energy* 2021; **6**: 339–48.
14. Holdcroft S. Fuel cell catalyst layers: a polymer science perspective. *Chem Mater* 2014; **26**: 381–93.
15. Wang J, Zhao Y and Setzler BP *et al.* Poly(aryl piperidinium) membranes and ionomers for hydroxide exchange membrane fuel cells. *Nat Energy* 2019; **4**: 392–8.
16. Kuroki H, Onishi K and Asami K *et al.* Catalyst slurry preparation using a hydrodynamic cavitation dispersion method for polymer electrolyte fuel cells. *Ind Eng Chem Res* 2019; **58**: 19545–50.
17. Cao H, Pan J and Zhu H *et al.* Interaction regulation between ionomer binder and catalyst: active triple-phase boundary and high performance catalyst layer for anion exchange membrane fuel cells. *Adv Sci* 2021; **8**: 2101744.
18. Buggy NC, Wu I and Du Y *et al.* Evaluating the effect of ionomer chemical composition in silver-ionomer catalyst inks toward the oxygen evolution reaction by half-cell measurements and water electrolysis. *Electrochim Acta* 2022; **412**: 140124.
19. Rabiee H, Ge L and Zhang X *et al.* Gas diffusion electrodes (GDEs) for electrochemical reduction of carbon dioxide, carbon monoxide, and dinitrogen to value-added products: a review. *Energy Environ Sci* 2021; **14**: 1959–2008.
20. Saha MS, Gullá AF and Allen RJ *et al.* High performance polymer electrolyte fuel cells with ultra-low Pt loading electrodes prepared by dual ion-beam assisted deposition. *Electrochim Acta* 2006; **51**: 4680–92.
21. Lee WH, Ko Y-J and Choi Y *et al.* Highly selective and scalable CO_2 to CO -electrolysis using coral-nanostructured Ag catalysts in zero-gap configuration. *Nano Energy* 2020; **76**: 105030.
22. Zhang G, Zhao ZJ and Cheng D *et al.* Efficient CO_2 electroreduction on facet-selective copper films with high conversion rate. *Nat Commun* 2021; **12**: 5745.
23. Jhong H-RM, Brushett FR and Kenis PJA. The effects of catalyst layer deposition methodology on electrode performance. *Adv Energy Mater* 2013; **3**: 589–99.
24. Marepally BC, Ampelli C and Genovese C *et al.* Role of small Cu nanoparticles in the behaviour of nanocarbon-based electrodes for the electrocatalytic reduction of CO_2. *J CO_2 Util* 2017; **21**: 534–42.
25. Tan YC, Lee KB and Song H *et al.* Modulating local CO_2 concentration as a general strategy for enhancing C−C coupling in CO_2 electroreduction. *Joule* 2020; **4**: 1104–20.
26. Fan J, Chen M and Zhao Z *et al.* Bridging the gap between highly active oxygen reduction reaction catalysts and effective catalyst layers for proton exchange membrane fuel cells. *Nat Energy* 2021; **6**: 475–86.
27. Ott S, Orfanidi A and Schmies H *et al.* Ionomer distribution control in porous carbon-supported catalyst layers for high-power and low Pt-loaded proton exchange membrane fuel cells. *Nat Mater* 2020; **19**: 77–85.
28. Berlinger SA, Chowdhury A and Van Cleve T *et al.* Impact of platinum primary particle loading on fuel cell performance: insights from catalyst/ionomer ink interactions. *ACS Appl Mater Interfaces* 2022; **14**: 36731–40.
29. Mowbray BAW, Dvorak DJ and Taherimakhsousi N *et al.* How catalyst dispersion solvents affect CO_2 electrolyzer gas diffusion electrodes. *Energy Fuels* 2021; **35**: 19178–84.
30. Avnir D. Recent progress in the study of molecularly doped metals. *Adv Mater* 2018; **30**: e1706804.
31. Soucy TL, Dean WS and Zhou J *et al.* Considering the influence of polymer-catalyst interactions on the chemical microenvironment of electrocatalysts for the CO_2 reduction reaction. *Acc Chem Res* 2022; **55**: 252–61.
32. Qin Y, Ji X and Jing J *et al.* Size control over spherical silver nanoparticles by ascorbic acid reduction. *Colloids Surf A* 2010; **372**: 172–6.
33. National Library of Medicine (US). *National Center for Biotechnology Information.* https://pubchem.ncbi.nlm.nih.gov/compound/Ascorbic-Acid (29 March 2023, date last accessed).
34. Bastús NG, Merkoçi F and Piella J *et al.* Synthesis of highly monodisperse citrate-stabilized silver nanoparticles of up to 200 nm: kinetic control and catalytic properties. *Chem Mater* 2014; **26**: 2836–46.
35. Ralbag N, Mann-Lahav M and Davydova ES *et al.* Composite materials with combined electronic and ionic properties. *Matter* 2019; **1**: 959–75.
36. Andrews LJ and Keefer RM. Cation complexes of compounds containing carbon–carbon double bonds. IV. The argentation of aromatic hydrocarbons. *J Am Chem Soc* 1949; **71**: 3644–7.
37. Endrődi B, Kecsenovity E and Samu A *et al.* High carbonate ion conductance of a robust PiperION membrane allows industrial current density and conversion in a zero-gap carbon dioxide electrolyzer cell. *Energy Environ Sci* 2020; **13**: 4098–105.
38. Reyes A, Jansonius RP and Mowbray BAW *et al.* Managing hydration at the cathode enables efficient CO_2 electrolysis at commercially relevant current densities. *ACS Energy Lett* 2020; **5**: 1612–8.
39. Endrodi B, Samu A and Kecsenovity E *et al.* Operando cathode activation with alkali metal cations for high current density operation of water-fed zero-gap carbon dioxide electrolyzers. *Nat Energy* 2021; **6**: 439–48.
40. Wheeler DG, Mowbray BAW and Reyes A *et al.* Quantification of water transport in a CO_2 electrolyzer. *Energy Environ Sci* 2020; **13**: 5126–34.
41. Romiluyi O, Danilovic N and Bell AT *et al.* Membrane-electrode assembly design parameters for optimal CO_2 reduction. *Electrochem Sci Adv* 2023; **3**: e2100186.
42. Rosen J, Hutchings GS and Lu Q *et al.* Mechanistic insights into the electrochemical reduction of CO_2 to CO on nanostructured Ag surfaces. *ACS Catal* 2015; **5**: 4293–9.
43. Ma M, Trześniewski BJ and Xie J *et al.* Selective and efficient reduction of carbon dioxide to carbon monoxide on oxide-derived nanostructured silver electrocatalysts. *Angew Chem Int Ed* 2016; **55**: 9748–52.
44. Guo SX, Bentley CL and Kang M *et al.* Advanced spatiotemporal voltammetric techniques for kinetic analysis and active site determination

in the electrochemical reduction of CO_2. *Acc Chem Res* 2022; **55**: 241–51.

45. Zhang X, Sun X and Guo S-X *et al.* Formation of lattice-dislocated bismuth nanowires on copper foam for enhanced electrocatalytic CO_2 reduction at low overpotential. *Energy Environ Sci* 2019; **12**: 1334–40.
46. Mariano RG, Kang M and Wahab OJ *et al.* Microstructural origin of locally enhanced CO_2 electroreduction activity on gold. *Nat Mater* 2021; **20**: 1000–6.
47. Bertei A, Ruiz-Trejo E and Kareh K *et al.* The fractal nature of the three-phase boundary: a heuristic approach to the degradation of nanostructured solid oxide fuel cell anodes. *Nano Energy* 2017; **38**: 526–36.
48. Ye S, Hou Y and Li X *et al.* Pore-scale investigation of coupled two-phase and reactive transport in the cathode electrode of proton exchange membrane fuel cells. *Trans Tianjin Univ* 2023; **29**: 1–13.
49. Wan Q, He Q and Zhang Y *et al.* Boosting the faradaic efficiency for carbon dioxide to monoxide on a phthalocyanine cobalt based gas diffusion electrode to higher than 99% via microstructure regulation of catalyst layer. *Electrochim Acta* 2021; **392**: 139023.
50. Xing Z, Hu X and Feng X. Tuning the microenvironment in gas-diffusion electrodes enables high-rate CO_2 electrolysis to formate. *ACS Energy Lett* 2021; **6**: 1694–702.
51. Xu Q, Oener SZ and Lindquist G *et al.* Integrated reference electrodes in anion-exchange-membrane electrolyzers: impact of stainless-steel gas-diffusion layers and internal mechanical pressure. *ACS Energy Lett* 2021; **6**: 305–12.
52. Cheng XC, Yi BL and Han M *et al.* Investigation of platinum utilization and morphology in catalyst layer of polymer electrolyte fuel cells. *J Power Sources* 1999; **79**: 75–81.
53. Yakovlev YV, Lobko YV and Vorokhta M *et al.* Ionomer content effect on charge and gas transport in the cathode catalyst layer of proton-exchange membrane fuel cells. *J Power Sources* 2021; **490**: 229531.